Automatic Tracking of Aponeuroses and Estimation of Muscle Thickness in Ultrasonography: A Feasibility Study

Shan Ling, Yongjin Zhou, Ye Chen, Yu-Qian Zhao, Lei Wang, and Yong-Ping Zheng, *Senior Member, IEEE*

***Abstract*—Muscle thickness measurement in ultrasonography was traditionally conducted by a trained operator, and the manual detecting process is time consuming and subjective. In this paper, we proposed an automatic tracking strategy to achieve the continuous and quantitative measurement for gastrocnemius muscle thickness in ultrasound images. The method involved three steps: tracking of seed points, contours extraction of aponeuroses, and muscle thickness estimation. In an ultrasound image sequence, we first selected two seed points in the first frame manually for the superficial and deep aponeuroses, respectively. Seed points in all following frames were then tracked by registering to their respective previous frames. Second, we adopted the local and global intensity fitting model to extract the contours of aponeuroses. At last, the muscle thickness was achieved by calculating the distance between the contours of superficial and deep aponeuroses. The performance of the algorithm was evaluated using 500 frames of ultrasound images. It was demonstrated in the experiments that the proposed methods could be used for objective tracking of aponeuroses and estimation of muscle thickness in musculoskeletal ultrasound images.**

Manuscript received November 12, 2012; revised February 7, 2013; accepted March 16, 2013. Date of publication March 21, 2013; date of current version November 12, 2013. This work was supported in part by the Hong Kong Innovation and Technology Commission under Grant GHP/047/09, the National 863 Program of China under Grant 2012AA02A604, the National 973 Program of China under Grant 2010CB732606, the next-generation communication technology Major project of National S&T under Grant 2013ZX03005013, the "Low-Cost Healthcare" Programs of Chinese Academy of Sciences, the Guangdong Innovative Research Team Program under Grant 2011S013, GIRTF-LCHT), and the International Science and Technology Cooperation Program of Guangdong Province under Grant 2012B050200004. Dr. Yongjin Zhou is the corresponding author.

S. Ling is with the Shenzhen Key Laboratory for Low-cost Healthcare, Shenzhen Institutes of Advanced Technology, Chinese Academy of Sciences, Shenzhen 518055, China, and also with the School of Geosciences and Info-Physics, Central South University, Changsha 410000, China.

Y. Zhou is with the Shenzhen Key Laboratory for Low-cost Healthcare, Shenzhen Institutes of Advanced Technology, Chinese Academy of Sciences, Shenzhen 518055, China, and also with the Interdisciplinary Division of Biomedical Engineering, The Hong Kong Polytechnic University, Hong Kong (e-mail: yj.zhou@siat.ac.cn), phone: 086-134-2866-6265; fax: 086-755-8639-2299.

Y. Chen is with the Shenzhen Key Laboratory for Low-cost Healthcare, Shenzhen Institutes of Advanced Technology, Chinese Academy of Sciences, Shenzhen 518055, China, and also with the School of Information Engineering, Nanchang Hangkong University, Nanchang 330000, China.

Y.-Q. Zhao is with the School of Geosciences and Info-Physics, Central South University, Changsha 410000, China.

L. Wang is with the Shenzhen Key Laboratory for Low-cost Healthcare, Shenzhen Institutes of Advanced Technology, Chinese Academy of Sciences, Shenzhen 518055, China.

Y.-P. Zheng is with the Interdisciplinary Division of Biomedical Engineering, The Hong Kong Polytechnic University, Hong Kong.

Color versions of one or more of the figures in this paper are available online at http://ieeexplore.ieee.org.

Digital Object Identifier 10.1109/JBHI.2013.2253787

***Index Terms*—Ultrasound imaging/ultrasonography, active contour, free-form deformation tracking, image registration, muscle thickness, sonomyography (SMG).**

I. Introduction

ULTRASOUND imaging has been employed to measure quantitative muscle changes in morphology, such as muscle thickness [1]–[6], muscle pennation angle [7]–[14], muscle fascicle length [2], [7], [15]–[17], and muscle cross-sectional area [7], [18]–[21] during contractions.

Muscle thickness is an important determinant of the muscle condition in many aspects. For example, Campbell *et al.* found that muscle thickness measured with ultrasound might be an indicator of lean tissue wasting in multiple organ failure in the presence of edema [1]. Miyatani *et al.* used muscle thickness to estimate the muscle volume of the quadriceps femoris based on ultrasonography [3]. Ohata *et al.* employed muscle thickness to quantify the muscle strength of people with severe cerebral palsy [5]. English *et al.* validated that ultrasound was a reliable measure of muscle thickness in acute stroke patients for some anatomical sites [22]. However, muscle thickness is traditionally measured by an experienced operator, and the process is not only subjective, but also time consuming. Recently, some researchers have presented several computer-aided methods, which could be used to estimate muscle thickness. Zheng *et al.* used sonomyography to describe the real-time change of muscle thickness detected using B-mode ultrasound images during its dynamic contraction [23] and proposed to use it for prosthetic control [20], [21]. Koo *et al.* used cross-correlation to track the locations of aponeuroses and measure muscle thickness on the ultrasound images [24]. They placed two windows on the superficial and deep aponeuroses and muscle thickness was calculated as the distance between the horizontal center lines of two windows. However, the line-shaped feature of aponeuroses would expose the cross-correlation tracking to risk of mismatches caused by feature self-similarity. It could be solved by constraining the cross-correlation tracking along the vertical direction only, supposing that the muscle hardly slides with respect to the ultrasound probe. Yet another more general problem with cross-correlation tracking is the choice of the matching template. The larger the template is, the more robust while less precise the tracking would be and *vice versa*. Wong *et al.* proposed a computerized system for measuring the thickness of the transverse abdominus, internal oblique, and external oblique muscles [6]. They performed ensemble

2168-2194 © 2013 IEEE

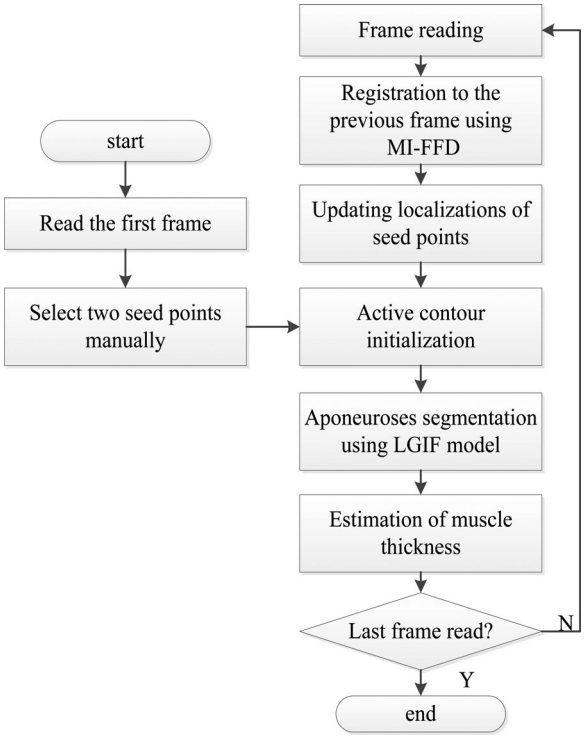

Fig. 1. Flowchart of the proposed strategy to measure GM thickness from one ultrasound image sequence. (MI-FFD for mutual information-based free-form deformation; LGIF for local and global intensity fitting.)

registration using a sequential quadratic programming approach based on a log-Rayleigh likelihood function and then identified regions of interest based on the medial border of the transverse abdominus. Although the muscle thickness was quantified automatically, the methods were based on measurements at several subjectively selected locations by nature, rather than the entire muscle boundary in ultrasound images. All of the aforementioned methods are limited to estimation of muscle thickness at one or several specific locations, assuming that the muscle thickness is constant longitudinally along the aponeuroses. But strictly speaking, superficial and deep aponeuroses are not straight lines, nor always parallel to each other, which leads to changes of muscle thickness at different longitudinal locations of aponeuroses.

In this paper, to compute muscle thickness of gastrocnemius (GM) in ultrasound images along the entire contours of aponeuroses, we proposed to extract the aponeuroses boundaries and calculate the distance between the lower boundary of superficial aponeurosis and upper boundary of deep aponeurosis as the muscle thickness.

II. Methods

The flowchart of the proposed strategy for muscle thickness measurement via ultrasonography is shown in Fig. 1. For each frame from the studied ultrasonography sequence, the first step was to acquire two seed points (one on the superficial aponeurosis, and the other on the deep aponeurosis). Then, contours of aponeuroses were extracted and muscle thickness was achieved by calculating the distance between contours of superficial and deep aponeuroses.

A. Tracking of Seed Points

In this paper, seed points in each frame are two points located on superficial and deep aponeuroses respectively, which will be used to generate initial contours in the aponeuroses segmentation stage. Given changes of muscle's shape and position in a sequence, locations of two seed points were adaptively adjusted in a frame-by-frame manner. However, considering the large number of images in a sequence, selecting seed points for every frame by hand is tedious and subjective. So we adopt an image registration method, named mutual information-based free-form deformation (MI-FFD) [25] tracking, to automatically track seed points in the ultrasound image sequence, since it produces local registration fields that are smooth, continuous and establish one-to-one correspondences. In this method, the transformation function which describes the deformation between two successive images is determined by minimizing a MI-based objective function. The derivation and details of the MI-FFD method can be found in Appendix I.

In summary, for each trial, seed points of the first frame are determined manually as two arbitrary points inside the contours of aponeuroses. For two consecutive frames of each sequence, the previous frame is selected as reference, and then, the MI-FFD method is applied to track the seed points in the subsequent frames automatically.

B. Aponeuroses Segmentation

Active contour models have been widely used in image segmentation with promising results since its introduction by Kass *et al.* [26]. In this paper, we adopt a region-based model, named the local and global intensity fitting (LGIF) model [27], to extract contours of aponeuroses, with the advantages of accuracy and robustness. In this model, an energy function is defined with a local intensity fitting term, which induces a local force to attract the contour and stops it at object boundaries, and an auxiliary global intensity fitting term, which drives the motion of the contour far away from object boundaries. The combination of these two forces can handle intensity inhomogeneity and allows for flexible initialization of the contours. Denoting ϕ as the level set function, the energy functional of the model is defined as

$$E(\phi) = (1-\omega) E_{\text{local}}(\phi) + \omega E_{\text{global}}(\phi) + \nu L(\phi) + \mu P(\phi) \tag{1}$$

where ω is a positive constant which determines the weight of the local force E_{local} and the global force E_{global}; $\nu > 0$ and $\mu > 0$ are constants as the weights of the length term $L(\phi)$ and the level set regularization term $P(\phi)$, respectively.

In this study, contours of each frame are initialized as two circles (radii $= 2$ pixels) centered at two seed points, which have been tracked by mean of MI-FFD described previously.

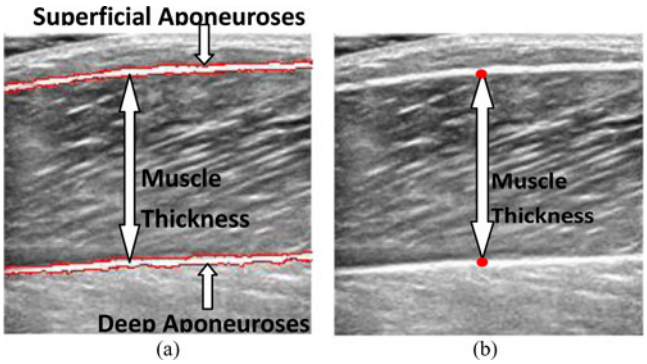

Fig. 2. Schematic diagrams of proposed strategy and manual method for muscle thickness measurement. (a) Our strategy for muscle thickness measurement. Muscle thickness was estimated by calculating the average distance between contours of superficial and deep aponeuroses. (b) Manual method for muscle thickness measurement. Muscle thickness was approximated as the distance between two points on lower edge of superficial aponeurosis and upper edge of deep aponeurosis, respectively.

Then, entire contours of aponeuroses will be extracted by evolving the level set iteratively using the LGIF model. The details and implementation of the LGIF model are introduced in Appendix II.

C. Estimation of Muscle Thickness

After segmentation of the aponeuroses, muscle thickness at each point along the aponeuroses is then estimated by calculating the distance between two corresponding points on superficial and deep aponeuroses, as shown in Fig. 2(a). Traditionally, muscle thickness is measured as the distance between two points, selected by an experienced operator, on the lower edge of superficial aponeurosis and the upper edge of deep aponeurosis respectively, as shown in Fig. 2(b). Therefore, to make comparison to the manual method, we additionally estimate the mean muscle thickness for each frame by calculating the mean distance between contours of superficial and deep aponeuroses, though our method outputs a curve of muscle thickness along the aponeuroses for each frame of ultrasound image.

III. Experiments

A. Subjects

Five healthy male subjects (mean $\pm$ SD, age $= 28.5 \pm 0.6$ years; body mass 67.3 ± 1.7 kg; height $= 171.8 \pm 0.6$ cm) volunteered to participate in this study. No participant had a history of neuromuscular disorders, and all were aware of experimental purposes and procedures. The human subject ethical approval was obtained from the relevant committee in the authors' institution, and informed consents were obtained from subjects prior to the experiment.

B. Experiment Protocol and Data Acquisition

The testing position of the subject was in accordance with the Users Guide of a Norm dynamometer (Humac/Norm Testing and Rehabilitation System, Computer Sports Medicine, Inc., Stoughton, MA, USA). Each subject was required to put forth his maximal effort of isometric plantar flexion for a period of 3 s with verbal encouragement provided. The maximal voluntary contraction (MVC) was defined as the highest value of torque recorded during the entire isometric contraction. The MVC torque was then calculated by averaging the two recorded highest torque values from the two tests. The subject was instructed to generate isometric plantar-flexion movements in prone position with angle of knee joint at 180°. The torque was measured by the aforementioned dynamometer and muscle contracting in a range from 0% to 90% MVC is imaged by ultrasonography. 90% MVC is set as the highest value to avoid muscle fatigue.

Fig. 3. Experimental setup for ultrasound image collection.

A real-time B-mode ultrasonic scanner (EUB-8500, Hitachi Medical Corporation, Tokyo, Japan) with a 10-MHz electronic linear array probe (L53L, Hitachi Medical Corporation, Tokyo, Japan) was used to obtain ultrasound images of muscles. The long axis of the ultrasound probe was arranged parallel to the long axis of the GM and on its muscle belly. The ultrasound probe was fixed by a custom-designed foam container with fixing straps, and a very generous amount of ultrasound gel was applied to secure acoustic coupling between the probe and skin during muscle contractions, as shown in Fig. 3. The probe was adjusted to optimize the contrast of muscle fascicles in ultrasound images. Then, the B-mode ultrasound images were digitized by a video card (NI PCI-1411, National Instruments, Austin, TX, USA) at a rate of 25 frames/s for later analysis.

C. Data Processing

Five sequences of musculoskeletal ultrasound images were acquired and the number of frames per sequence was 100 images. All images were cropped to remove imaging tags and kept the image content only using home-made software. All data were processed offline using programs written in MATLAB R 2010b (Math Works, Natick, MA, USA) on a Windows-based computer with a P4 (3 GHz) processor and 8-GB memory.

IV. Results

A. Seed Points Tracking

A representative example of the procedure for seed points tracking is shown in Fig. 4. Fig. 4(a) shows the current frame of one image sequence whose seed points has been determined,

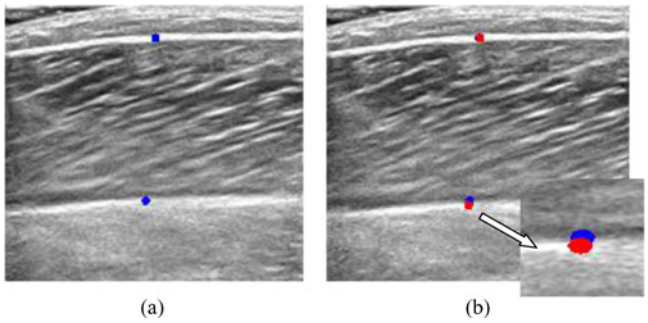

Fig. 4. Representative example of the procedure for seed points tracking. (a) One frame of a sequence with manually selected seed points represented by two blue points. (b) Subsequent frame, where red points are true seed points determined by MI-FFD method and blue points are at the same position as in (a). MI-FFD stands for mutual-information-based free-form deformation.

as represented by the two blue points in the figure. Seed points of the subsequent frame in the sequence are shown in Fig. 4(b), where red points are true seed points determined by MI-FFD method and blue points are at the same position as Fig. 4(a). It can be seen that the method can update positions of seed points back onto aponeuroses when the muscle contracted and location of aponeuroses changes accordingly.

B. Aponeuroses Segmentation

In our numerical experiments for aponeuroses segmentation using the LGIF model, we empirically adopted parameters as follows: $\lambda_1 = \lambda_2 = 1.0, \nu = 0.001 \times 255 \times 255, \mu = 1, \omega = 0.01, \sigma = 3.0$, and time step $t = 0.23$, where λ_1 and λ_2 are parameters of the intrinsic energy function, and σ is the standard deviation (SD) of the Gaussian kernel. Detailed information about these parameters can be found in Appendix II. Simply speaking, the larger σ or t is, the sooner the methods would converge, meanwhile more exposed to risk of trapped by less accurate or wrong features.

A representative example of aponeuroses segmentation process using LGIF evolution model is shown in Fig. 5.

C. Muscle Thickness Measurement

Our strategy proposed in this paper has the ability to measure muscle thickness along the entire contours of aponeuroses, so we can get a curve of muscle thickness for each frame of ultrasound image. Muscle thickness of a representative frame estimated by our method is shown in Fig. 6.

Estimation of the mean muscle thickness for each frame was additionally made by calculating the mean distance between contours of superficial and deep aponeuroses, for the purpose to make the comparison to the manual method. A representative result of muscle thickness of the whole image sequence, measured by the proposed technique and the manual method, is displayed in Fig. 7. To further quantitatively evaluate our algorithm, we define the thickness error rate (TER) to compare muscle thickness measured by the proposed strategy (PT) and the manual method (MT) as

$$\mathrm{TER} = |(\mathrm{PT} - \mathrm{MT})/\mathrm{MT}| \times 100\%. \quad (2)$$

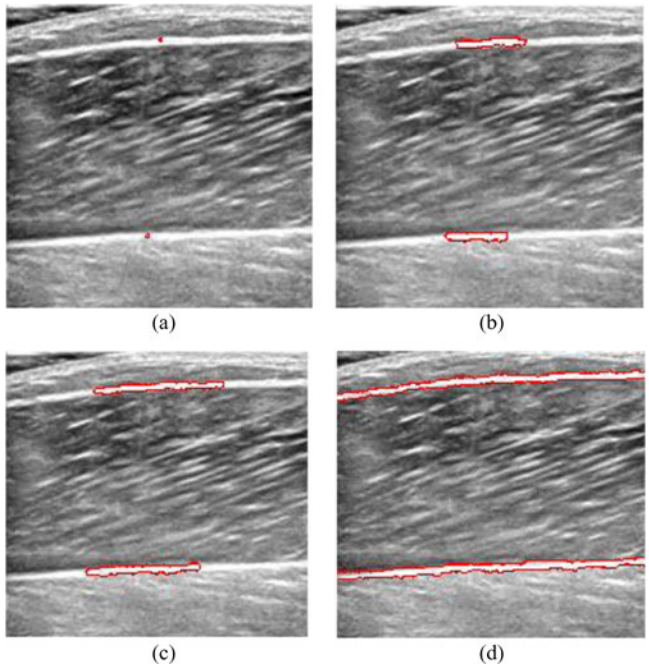

Fig. 5. Representative set of results of the LGIF model for aponeuroses segmentation. (a) Original image with initial contour. (b) Curve evolution result after 50 iterations. (c) Curve evolution result after 300 iterations. (d) Final contour after evolving stopped.

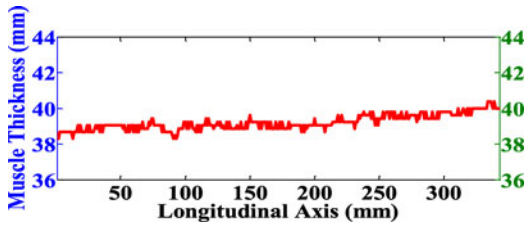

Fig. 6. Muscle thickness estimated along the entire longitudinal axis of a representative frame.

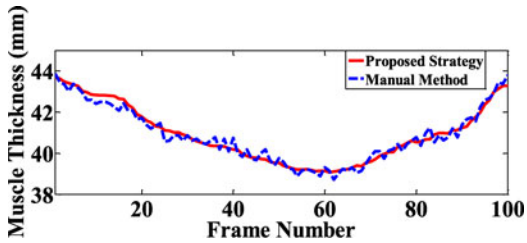

Fig. 7. Representative comparison result of muscle thickness measured by our strategy and manual technique.

The average thickness and TER measured for all subjects are listed in Table I.

To further investigate the performance of the proposed strategy, interframe differences of MT and PT curves for a representative subject are compared in Fig. 8. Detailed quantitative results are also listed in Table II. It should also be noted that, in addition to measurement of the muscle, the thickness of superficial and deep aponeuroses can also be estimated readily by calculating the width of their contours. Fig. 9 shows the thickness measurements of superficial aponeuroses in a representative

TABLE I
MUSCLE THICKNESS MEASURED BY THE PROPOSED STRATEGY (PT) AND THE MANUAL METHOD (MT), AND THICKNESS ERROR RATE (TER) MEASURED FOR ALL SUBJECTS

Subject	Muscle Thickness (mm)		TER (%)
	PT	MT	
1	39.3±1.2	38.8±1.2	1.2±0.8
2	41.1±1.4	41.0.±1.6	0.8±0.6
3	40.9±1.4	40.9±1.4	0.5±0.4
4	40.0±1.5	40.0±1.5	0.6±0.4
5	47.5±0.6	46.9±0.7	1.4±0.5

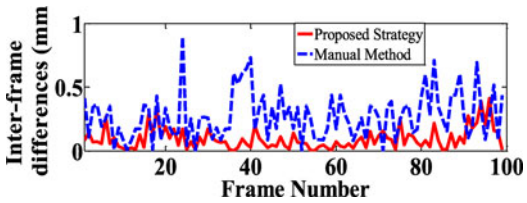

Fig. 8. Interframe differences of muscle thickness measured by the manual method and proposed strategy for a representative subject.

TABLE II
INTERFRAME DIFFERENCES OF MUSCLE THICKNESS MEASURED BY MANUAL METHOD (MT) AND PROPOSED STRATEGY (PT) FOR ALL SUBJECTS

Subject	Inter-frame differences (mm)	
	MT	PT
1	0.3±0.2	0.1±0.1
2	0.3±0.3	0.1±0.1
3	0.3±0.2	0.1±0.1
4	0.3±0.2	0.1±0.1
5	0.2±0.1	0.1±0.1

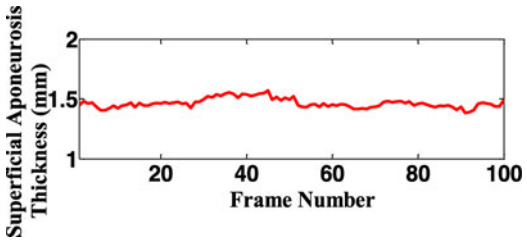

Fig. 9. Superficial aponeuroses thickness of a representative frame measured by the proposed strategy.

image sequence and thickness measurements of superficial aponeuroses from all subjects are listed in Table III.

V. DISCUSSION

Previous studies for muscle thickness measurement using either manual or computer-aided methods, estimate muscle thickness at one or several locations, ignoring the fact that muscle thickness changes longitudinally along aponeuroses. It can be seen from Fig. 6 that muscle thickness is not constant along the aponeuroses. Therefore, a new strategy was proposed to estimate muscle thickness for each point along the longitudinal axis of the ultrasound image based on extracting contours of aponeuroses, which would be very useful when interested in muscle thickness at more than one or several specific locations.

TABLE III
THICKNESS MEASUREMENTS OF SUPERFICIAL APONEUROSES FROM ALL SUBJECTS

Subject	Thickness of Superficial Aponeuroses (mm)
1	1.5±0.0
2	1.5±0.0
3	1.6±0.1
4	1.5±0.1
5	1.4±0.1

To evaluate the validity of our strategy, we additionally averaged muscle thickness of the frame by calculating the mean distance between superficial and deep aponeuroses, and made comparison with the measurement result of manual method. As shown in Fig. 7, it is found in the experiments that this mean muscle thickness, derived from the results generated using the proposed strategy, agrees well with the manual results. Meanwhile, it can be observed in Table I that the proposed strategy shows good performance with maximal TER of 1.35%. The average TER value for all images is 0.87%. The differences are inevitable since MT calculates only the distance between two selected points, while PT calculates the mean distance between contours of aponeuroses. In practice, the muscle thickness can change slightly along longitudinal axis of the ultrasound image, as shown in Fig. 6.

For consecutive ultrasound images captured during muscle contraction, location of aponeuroses in a specific frame should not change much from neighboring frames. Therefore, it is expected to see that muscle thickness only change slightly across frames. It can be seen that PT exhibited much smaller fluctuations than MT in Fig. 7. As shown in Fig. 8 and Table II, for the results from a representative subject, PT provided a higher level of measurement stability with lower interframe difference. Given the fact that change of aponeuroses width in a sequence is trivial, the SD of thickness of superficial aponeurosis itself in a sequence could indirectly reflect the error level of our strategy. From Fig. 9 and Table III, it can be observed that the thickness of superficial aponeurosis is almost constant and SDs from all subjects are 0.1 ± 0.0 mm or 0.3 ± 0.1 pixels, which can serve as an indirect proof that the error level of the proposed method was no larger than 0.1 mm.

The proposed methods work well under isometric contraction because muscle sliding under this condition should be minimal. However, during joint motion, the relative motion of the muscles to the skin surface could change the portion of the muscle being imaged. This may affect the muscle thickness measurement. In addition, if the transducer is not positioned such that the aponeuroses run along the horizontal direction of the ultrasound image, the thickness measurement could increase substantially, therefore in our study, the ultrasound probe was fixed by a custom-designed foam container with fixing straps to force the probe remain in the same vertical imaging plane. However, when the muscle belly bulged, the probe could be pushed away slightly. Both problems are also general for all sonography studies (either manual or automatic) on muscle contractions. We would like to point out that all data in current report are all collected

from young and healthy subjects. More data are planned to be collected from subjects with musculoskeletal disorders covering a wider age range to test and further improve the methods.

VI. Conclusion

In this paper, we present a new strategy for the measurement of muscle thickness along the entire length of aponeuroses in ultrasonography, which is useful when curvature of aponeuroses and longitudinal variance of muscle thickness are unnegligible. Results of the experiments suggest that the proposed strategy can be used for objective estimation of muscle thickness in musculoskeletal ultrasound images.

Appendix I

The MI-FFD method, originally proposed in [25] to do shape registration based on the MI between two images, was applied in this paper for frame registration and seed points tracking. The similarity criterion and transformation model of the method adopted in this method were MI and B-spline FFD, respectively.

The essence of FFD is to deform the shape of an object by manipulating a regular control lattice P overlaid on its volumetric embedding space. A dense deformation field for every pixel in the embedding space can be acquired through interpolation using an interpolating basis function, such as Bezier spline or B-spline functions [25]. In this method, the deformation function T is defined by a 2-D spline function, which is parameterized by displacement vectors at a uniform grid of control points.

Let P be a uniform grid of control points

$$P=\{P_{m,n}\}=\left\{\left(P^x_{m,n},P^y_{m,n}\right)\right\},m=1,\ldots,M,n=1,\ldots,N \tag{A1}$$

overlaid to an image domain A, and the size of A is $X\times Y$. The spacing of the grid P in the $\vec{x}$ and $\vec{y}$ directions are $n_x = X/M$ and $n_y = Y/N$. Then, FFD parameters are deformation improvements of control points in both $\vec{x}$- and $\vec{y}$-directions

$$\theta=\delta P=\left\{\left(\delta P^x_{m,n},\delta P^y_{m,n}\right)\right\};(m,n)\in[1,M]\times[1,N]. \tag{A2}$$

So, the transformation function $T(x,y)$ is defined by a tensor product of cubic B-splines

$$T(x,y)=\sum_{l=0}^{3}\sum_{k=0}^{3}B_l(u)\,B_k(v)\,P_{i+l.j+k} \tag{A3}$$

where $i=\lfloor x/n_x\rfloor-1, j=\lfloor y/n_y\rfloor-1, u=x/n_x-\lfloor x/n_x\rfloor$, $v=y/n_y-\lfloor y/n_y\rfloor$, and B_l is the lth cubic B-spline basic function.

After the transformation of the floating image, we will compute MI between the transformed image and reference image. Then, parameters θ of the transformation function $T(\cdot)$ will be optimized by maximizing MI.

In probability theory and information theory, the MI of two random variables is a quantity that measures the mutual dependence of the two random variables. Here, we introduce two random variables A and B denoting reference image and floating image respectively. Image B is then deformed by mean of a transformation function $T(\cdot)$ with parameters to be determined by maximizing the MI between A and $T(B)$. The MI between the two images can be defined as [25]

$$\begin{aligned}MI(A;T(B))&=H(A)+H(T(B))-H(A,T(B))\\&=\sum_{b\in T(B)}\sum_{a\in T(A)}P(a,b)\log\left(P(a,b)/(P(a)\,P(b))\right)\end{aligned} \tag{A4}$$

where $H(A)$, $H(T(B))$, and $H(A,T(B))$ are the entropies of reference image A, transformed image $T(B)$, and their joint entropy, respectively; $P(a)$ and $P(b)$ represent intensity probability distribution functions of A and $T(B)$, respectively; and $P(a,b)$ is their joint probability distribution function.

Therefore, by minimizing the objective function $E=-\mathrm{MI}$, using parameters of transformation function $T(\cdot)$, the two original images can be registered and initial seed points can be tracked continuously.

In this paper, we adopted the Limited-memory Broyden–Fletcher–Goldfarb–Shanno (L-BFGS) algorithm [28] as the optimization method to search optimal transformation parameters which could be minimize the object function E. An advantage of the L-BFGS algorithm is that the explicit evaluation of the Hessian matrix is not required, so it can be recursively estimated. Moreover, the L-BFGS algorithm is much faster than the conventional level set method for solving the nonlinear optimization problem.

Appendix II

The LGIF model [27] combines advantages of the Chan–Vese (CV) model [29] and the local binary fitting (LBF) model [30] by taking the local and global intensity information into account. The gradient decent flow equation of the LGIF energy function is defined as [27]

$$\begin{aligned}\partial\phi/\partial t=\delta(\phi)(F_1+F_2)+\nu\delta(\phi)\,div(\nabla\phi/|\nabla\phi|)\\+\mu\left(\nabla^2\phi-div(\nabla\phi/|\nabla\phi|)\right)\end{aligned} \tag{B1}$$

where δ is the 1-D Dirac function. F_1 is the component of LBF model which was proposed to segment images with intensity inhomogeneity, and F_2 is the component of the CV model. Given the image $I(\mathbf{x})(\mathbf{x}:(x,y),1\le x\le X,1\le y\le Y)$ to be segmented, F_1 and F_2 can be formulated as [27]

$$\begin{aligned}F_1=(1-\omega)[-\lambda_1\textstyle\int K_\sigma(\mathbf{y}-\mathbf{x})\,|I(\mathbf{x})-f_1(\mathbf{y})|^2\,d\mathbf{y}\\+\lambda_2\textstyle\int K_\sigma(\mathbf{y}-\mathbf{x})\,|I(\mathbf{x})-f_2(\mathbf{y})|^2\,d\mathbf{y}]\end{aligned} \tag{B2}$$

$$F_2=\omega\left[-\lambda_1|I(\mathbf{x})-c_1|^2+\lambda_2|I(\mathbf{x})-c_2|^2\right] \tag{B3}$$

where λ_1 and λ_2 are nonnegative constants, and ω is a positive constant ($0\le\omega\le1$). When images are corrupted by intensity inhomogeneity, the parameter value ω should be chosen small enough. K_σ is a Gaussian kernel with SD σ. c_1 and c_2 are two constants that approximate the image intensity in the regions outside and inside the contour which are expressed in the following way [29]:

$$\begin{aligned}c_1&=\int I(\mathbf{x})H(\phi(\mathbf{x}))\mathbf{dx}\Big/\int H(\phi(\mathbf{x}))\,\mathbf{dx}\\c_2&=\int I(\mathbf{x})(1-H(\phi(\mathbf{x})))\,\mathbf{dx}\Big/\int(1-H(\phi(\mathbf{x})))\,\mathbf{dx}\end{aligned} \tag{B4}$$

where H is 1-D Heaviside function. In contrast to the two constants c_1 and c_2, functions f_1 and f_2 are spatially varying fitting functions [30]

$$f_1(\mathbf{x}) = K_\sigma(\mathbf{x}) [H(\phi(\mathbf{x})) I(\mathbf{x})] / [K_\sigma(\mathbf{x}) H(\phi(\mathbf{x}))]$$
$$f_2(\mathbf{x}) = K_\sigma(\mathbf{x}) [(H(\phi(\mathbf{x}))) I(\mathbf{x})] / [K_\sigma(\mathbf{x}) (1 - H(\phi(\mathbf{x})))]. \tag{B5}$$

In practice, Heaviside function H is approximated by a smooth function H_ε defined by

$$H_\varepsilon(\mathbf{x}) = [1 + (2 \arctan(\mathbf{x}/\varepsilon))/\pi]/2 \tag{B6}$$

where ε is a positive constant. The derivative of H_ϵ is the smoothed Dirac delta function

$$\delta_\varepsilon(\mathbf{x}) = \varepsilon / [\pi(\varepsilon^2 + \mathbf{x}^2)]. \tag{B7}$$

The parameter ε in H_ε and δ_ε is set to 1.0. This parameter can be fixed as this value in practice.

In this study, to reduce the number of iterations, contours are initialized as two circles centered at two seed points. In our implementation, assuming the coordinates of the two seed points are $(x_1, y_1), (x_2, y_2)$, respectively, then contours are initialized as $\phi_0 = [\phi_{1,0}; \phi_{2,0}]$, where

$$\begin{cases} \phi_{1,0}(\mathbf{x}) = \sqrt{(x - x_1)^2 + (y - y_1)^2} - 2, \\ \phi_{2,0}(\mathbf{x}) = \sqrt{(x - x_2)^2 + (y - y_2)^2} - 2, \end{cases}$$
$$(0 \le x \le X, 0 \le y \le Y/2). \tag{B8}$$

Finally, the principle steps of the LGIF algorithm are as follows.

1) Set parameters $\lambda_1, \lambda_2, \omega, \nu, \mu$, and time step Δt;
2) Initialize ϕ^0 by $\phi_0, n = 0$;
3) Compute $F_1(\phi^n)$ and $F_2(\phi^n)$ by (A4) and (B1);
4) Obtain $\phi^{n+1} = \phi^n + \Delta t(\partial\phi/\partial t)$, according to (A3);
5) Check whether the solution is stationary. If not, $n = n + 1$ and repeat.

REFERENCES

[1] T. W. lain, T. Campbell, D. Withers, R. England, S. Sukumar, M. A. Keegan, B. Faragher, and D. F. Martin, "Muscle thickness, measured with ultrasound, may be an indicator of lean tissue wasting in multiple organ failure in the presence of edema1," *Amer. Soc. Clin. Nutrition*, vol. 62, pp. 533–539, 1995.

[2] G. Misuri, S. Colagrande, M. Gorini, I. Iandelli, M. Mancini, R. Duranti, and G. Scano, "In vivo ultrasound assessment of respiratory function of abdominal muscles in normal subjects," *Eur. Respiratory J.*, vol. 10, pp. 2861–2867, 1997.

[3] H. K. Masae Miyatani, A. Kuno, T. Nishijima, and T. Fukunaga, "Validity of ultrasonograph muscle thickness measurements for estimating muscle volume of knee extensors in humans," *Eur. J. Appl. Phys.*, vol. 86, pp. 203–208, 2002.

[4] P. W. Hodges, "Measurement of muscle contraction with ultrasound imaging," *Muscle Nerve*, vol. 27, pp. 682–692, 2003.

[5] K. Ohata, T. Tsuboyama, N. Ichihashi, and S. Minami, "Measurement of muscle thickness as quantitative muscle evaluation for adults with severe cerebral palsy," *Phys. Ther.*, vol. 86, pp. 1231–9, Sep. 2006.

[6] A. Wong, K. M. Gallagher, and J. P. Callaghan, "Computerised system for measurement of muscle thickness based on ultrasonography," *Comput. Methods Biomech. Biomed. Eng.*, Feb. 29, 2012.

[7] M. Narici, T. Binzoni, E. Hiltbrand, J. Fasel, F. Terrier, and P. Cerretelli, "In vivo human gastrocnemius architecture with changing joint angle at rest and during graded isometric contraction," *J. Phys.*, vol. 496, pp. 287–297, 1996.

[8] T. Fukunaga, Y. Ichinose, M. Ito, Y. Kawakami, and S. Fukashiro, "Determination of fascicle length and pennation in a contracting human muscle in vivo," *J. Appl. Phys.*, vol. 82, pp. 354–358, 1997.

[9] M. Ito, Y. Kawakami, Y. Ichinose, S. Fukashiro, and T. Fukunaga, "Nonisometric behavior of fascicles during isometric contractions of a human muscle," *J. Appl. Phys.*, vol. 85, pp. 1230–1235, 1998.

[10] C. N. Maganaris, V. Baltzopoulos, and A. J. Sargeant, "Repeated contractions alter the geometry of human skeletal muscle," *J. Appl. Phys.*, vol. 93, pp. 2089–2094, 2002.

[11] Y. Zhou and Y. P. Zheng, "Estimation of muscle fiber orientation in ultrasound images using revoting hough transform (RVHT)," *Ultrasound Med. Biol.*, vol. 34, pp. 1474–1481, 2008.

[12] Y. Zhou and Y. P. Zheng, "Longitudinal enhancement of the hyperechoic regions in ultrasonography of muscles using a Gabor filter bank approach: A preparation for semi-automatic muscle fiber orientation estimation," *Ultrasound Med. Biol.*, vol. 37, pp. 665–673, 2011.

[13] H. Zhao and L. Q. Zhang, "Automatic tracking of muscle fascicles in ultrasound images using localized radon transform," *IEEE Trans. Biomed. Eng.*, vol. 58, no. 7, pp. 2094–2101, Jul. 2011.

[14] Y. Zhou, J. Li, G. Zhou, and Y. Zheng, "Dynamic measurement of pennation angle of gastrocnemius muscles during contractions based on ultrasound imaging," *Biomed. Eng. Online*, vol. 11, 2012. [Online]. doi: 10.1186/1475-925X-11-63.

[15] L. Mademli and A. Arampatzis, "Behaviour of the human gastrocnemius muscle architecture during submaximal isometric fatigue," *Eur. J. Appl. Phys.*, vol. 94, pp. 611–617, 2005.

[16] G. A. Lichtwark, K. Bougoulias, and A. Wilson, "Muscle fascicle and series elastic element length changes along the length of the human gastrocnemius during walking and running," *J. Biomech.*, vol. 40, pp. 157–164, 2007.

[17] J. G. Gillett, R. S. Barrett, and G. A. Lichtwark, "Reliability and accuracy of an automated tracking algorithm to measure controlled passive and active muscle fascicle length changes from ultrasound," *Comput. Methods Biomech. Biomed. Eng.*, Jan. 11, 2012. [Online]. doi:10.1080/10255842.2011.633516.

[18] N. D. Reeves, C. N. Maganaris, and M. V. Narici, "Ultrasonographic assessment of human skeletal muscle size," *Eur. J. Appl. Phys.*, vol. 91, pp. 116–118, 2004.

[19] C. N. Maganaris, V. Baltzopoulos, and A. J. Sargeant, "Human calf muscle responses during repeated isometric plantar flexions," *J. Biomech.*, vol. 39, pp. 1249–1255, 2006.

[20] J. Y. Guo, Y. P. Zheng, H. B. Xie, and X. Chen, "Continuous monitoring of electromyography (EMG), mechanomyography (MMG), sonomyography (SMG) and torque output during ramp and step isometric contractions," *Med. Eng. Phys.*, vol. 32, pp. 1032–1042, 2010.

[21] X. Chen, Y. P. Zheng, J. Y. Guo, Z. Zhu, S. C. Chan, and Z. Zhang, "Sonomyographic responses during voluntary isometric ramp contraction of the human rectus femoris muscle," *Eur. J. Appl. Phys.*, vol. 112, pp. 2603–2614, 2011.

[22] C. K. English, K. A. Thoirs, L. Fisher, H. McLennan, and J. Bernhardt, "Ultrasound is a reliable measure of muscle thickness in acute stroke patients, for some, but not all anatomical sites: A study of the intra-rater reliability of muscle thickness measures in acute stroke patients," *Ultrasound Med. Biol.*, vol. 38, pp. 368–376, 2012.

[23] Y. P. Zheng, M. Chan, J. Shi, X. Chen, and Q. H. Huang, "Sonomyography: Monitoring morphological changes of forearm muscles in actions with the feasibility for the control of powered prosthesis," *Med. Eng. Phys.*, vol. 28, pp. 405–415, 2006.

[24] T. K. K. Koo, C. Wong, and Y. Zheng, "Reliability of sonomyography for pectoralis major thickness measurement," *J. Manipulative Physiol. Therapeutics*, vol. 33, pp. 386–394, 2010.

[25] X. Huang, N. Paragios, and D. N. Metaxas, "Shape registration in implicit spaces using information theory and free form deformations," *IEEE Trans. Pattern Anal. Mach. Intell.*, vol. 28, no. 8, pp. 1303–1318, Aug. 2006.

[26] M. Kass, A. Witkin, and D. Terzopoulos, "Snakes: Active contour models," *Int. J. Comput. Vis.*, vol. 1, pp. 321–331, 1988.

[27] L. Wang, C. Li, Q. Sun, D. Xia, and C. Y. Kao, "Active contours driven by local and global intensity fitting energy with application to brain MR image segmentation," *Comput. Med. Imag. Graph.*, vol. 33, pp. 520–31, Oct. 2009.

[28] R. H. Byrd, P. Lu, J. Nocedal, and C. Zhu, "A limited memory algorithm for bound constrained optimization," *SIAM J. Sci. Comput.*, vol. 16, pp. 1190–1208, 1995.

[29] T. F. Chan and L. A. Vese, "Active contours without edges," *IEEE Trans. Image Process.*, vol. 10, no. 2, pp. 266–277, Feb. 2001.

[30] C. Li, C. Y. Kao, J. C. Gore, and Z. Ding, "Implicit active contours driven by local binary fitting energy," in *Proc. IEEE Conf. Comput. Vision Pattern Recog.*, 2007, pp. 1–7.

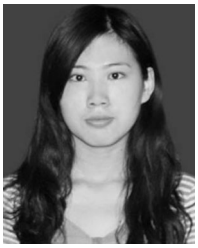

Shan Ling was born in China in 1989. She is currently working toward the M.S. degree at Central South University, Hunan, China, and studying as a visiting student at the Shenzhen Institute of advanced technology, Shenzhen, China.

Her research interests include medical image processing and pattern recognition.

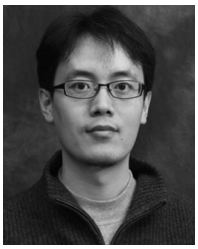

Yongjin Zhou was born in China in 1975. He received the B.Sc., M.Eng., and Ph.D. degrees in biomedical engineering from Xi'an Jiaotong University, Xi'an, China, in 1996, 1999, and 2003, respectively.

After a postdoctoral fellowship at the Oregon Hearing Research Center, Portland, USA, working on nonlinear signal analysis, modeling, and pattern recognition, he joined Hong Kong Polytechnic University, Hong Kong, in 2005, and worked there until 2012. He is currently an Associate Professor in the Shenzhen Institutes of Advanced Technology, Chinese Academy of Sciences, Beijing, China. His research interests include biological signal processing, medical ultrasound, medical image analysis, and pattern recognition.

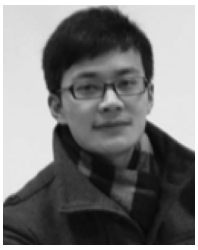

Ye Chen was born in China in 1988. He is currently working toward the M.S. degree in electrical and communication engineering from Nanchang Hangkong University, Nanchang, China.

His research interests mainly include image processing and computer vision.

Yu-Qian Zhao received the Ph.D. degree from Central South University, Changsha, China, in 2006.

He was a Postdoctoral Researcher at the Xiangya School of Medicine, China, from May 2007 to June 2009, and New Jersey Institute of Technology, Newark, USA, from July 2009 to July 2010. He is currently a Professor in the Institute of Biomedical Engineering, Central South University. His research interests include image and video processing, pattern recognition, computer vision, image forensics, and computer-aided diagnosis.

Lei Wang received the B.Eng. degree in information and control engineering and the Ph.D. degree in biomedical engineering from Xi'an Jiaotong University, China, in 1995 and 2000, respectively.

He was with the University of Glasgow and the Imperial College London during 2000–2008. He is currently a Full Professor with the Shenzhen Institutes of Advanced Technology, Chinese Academy of Sciences, Beijing, China. He has published more than 200 scientific papers, authored four book chapters, and filed 60 patents. His research interests focus on body sensor network.

Yong-Ping Zheng (SM'06) received the B.Sc. and M.Eng. degrees in electronics and information engineering from the University of Science and Technology of China, Hefei, China, and the the Ph.D. degree in biomedical engineering from the Hong Kong Polytechnic University (PolyU), Hong Kong, in 1997.

After a postdoctoral fellowship at the University of Windsor, Windsor, ON, Canada, he joined PolyU as an Assistant Professor in 2001 and was prompted to Associate Professor and Professor in 2005 and 2008, respectively. He served as the Associate Director of the Research Institute of Innovative Products in PolyU from 2008 to 2010. He is currently serving as the Acting Head of the newly established Interdisciplinary Division of Biomedical Engineering and a member of PolyU Knowledge Transfer Committee. As Chief Supervisor, he has trained six Postdoctoral Fellows, seven Ph.D., six M.Phil graduates, and four Ph.D. students are currently under his supervision. His main research interests include biomedical ultrasound instrumentation, 3-D ultrasound imaging, tissue elasticity measurement and imaging, and wearable sensors for healthcare. He holds seven U.S. and ten Chinese patents and has other eight patents pending, in the field of biomedical ultrasound and wearable sensors. Nine of these patents have been successfully licensed to industry for commercialization.

Dr. Zheng is on the Editorial Boards of a number of journals, including *Ultrasound in Medicine and Biology*, *International Advisory Board of Physiological Measurement*, and the Associate Editor of *Transactions of Hong Kong Institution of Engineers*. He received international awards for a number of his research and development works.